Journal of Colloid and Interface Science 628 (2022) 486–498

Contents lists available at ScienceDirect

Journal of Colloid and Interface Science

journal homepage: www.elsevier.com/locate/jcis

Pore-scale processes in tertiary low salinity waterflooding in a carbonate rock: Micro-dispersions, water film growth, and wettability change

Ahmed M. Selem [a], Nicolas Agenet [b], Martin J. Blunt [a], Branko Bijeljic [a]

[a] Department of Earth Science and Engineering, Imperial College London, SW7 2AZ London, United Kingdom
[b] TotalEnergies, Pau, France

GRAPHICAL ABSTRACT

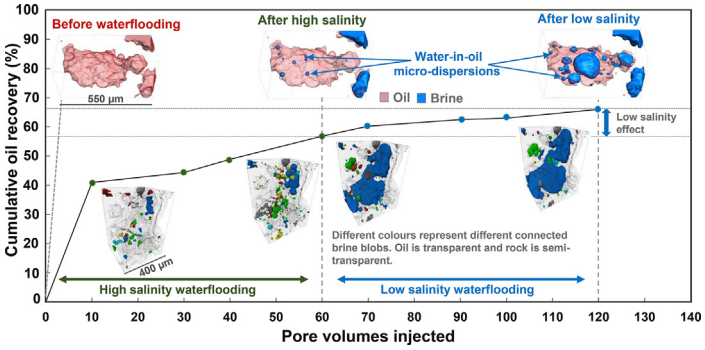

ARTICLE INFO

Article history:
Received 10 February 2022
Revised 6 June 2022
Accepted 14 June 2022
Available online 18 June 2022

Keywords:
Low salinity waterflooding
Pore-scale mechanisms
Enhanced oil recovery
Micro-dispersions
Wettability change
X-ray micro-CT coreflooding

ABSTRACT

Hypothesis: The wettability change from oil-wet towards more water-wet conditions by injecting diluted brine can improve oil recovery from reservoir rocks, known as low salinity waterflooding. We investigated the underlying pore-scale mechanisms of this process to determine if improved recovery was associated with a change in local contact angle, and if additional displacement was facilitated by the formation of micro-dispersions of water in oil and water film swelling.

Experiments: X-ray imaging and high-pressure and temperature flow apparatus were used to investigate and compare high and low salinity waterflooding in a carbonate rock sample. The sample was placed in contact with crude oil to obtain an initial wetting state found in hydrocarbon reservoirs. High salinity brine was then injected at increasing flow rates followed by low salinity brine injection using the same procedure.

Findings: Development of water micro-droplets within the oil phase and detachment of oil layers from the rock surface were observed after low salinity waterflooding. During high salinity waterflooding, contact angles showed insignificant changes from the initial value of 115°, while the mean curvature and local capillary pressure values remained negative, consistent with oil-wet conditions. However, with low salinity, the decrease in contact angle to 102° and the shift in the mean curvature and capillary pressure to positive values indicate a wettability change. Overall, our analysis captured the *in situ* mechanisms and processes associated with the low salinity effect and ultimate increase in oil recovery.

https://doi.org/10.1016/j.jcis.2022.06.063
0021-9797/

1. Introduction

Carbonate reservoirs are essential in the energy sector as they contain most of the world's remaining hydrocarbon reserves [1]. However, it is challenging to understand extraction processes due to the complex interplay between pore structure and wettability. For example, waterflooding is widely implemented in oil fields to maintain reservoir pressure and improve oil recovery [2]. Typically high salinity brine is used in this process; however, this may leave a significant amount of oil in the reservoir [3]. Therefore, additional research has been focused on finding ways to improve the efficiency of waterflooding. It has been shown that waterflooding could recover more oil when the brine's salinity or composition is changed [4] through the process known as low salinity waterflooding (LSW). A screening study performed on several oil fields in the Norwegian continental shelf highlighted the potential of LSW as one of the key enhanced oil recovery (EOR) methods based on technical, operational, environmental and economic criteria [5].

Previous experimental work on low salinity waterflooding showed that reducing brine salinity could cause changes induced by physio-chemical mechanisms in sandstone [6–12] and carbonate rocks [13–19], increasing the oil recovery factor. Field trials have reinforced these findings [3,9,20–22]. The change in the rock surface wettability from oil-wet to a more water-wet state is considered the primary mechanism for the incremental increase in oil recovery [23–27]. However, the wettability shift could be driven by different underlying pore-scale processes and mechanisms, which are yet to be explored and understood [28].

Fluid-fluid and fluid-solid interactions are critical in the low salinity effect (LSE), especially at the pore scale. Oftentimes, effects induced by salinity concentration gradients and water-oil emulsions are not given the same consideration as other processes during low salinity waterflooding studies [28–30]. However, these effects have the potential to change the rock wettability and mobilize oil over a relatively short period of a few days. Osmosis and water-in-oil emulsions have been proposed as the main underlying mechanisms for the LSE [26,31–36]. The higher the tendency of a certain oil to form micro-dispersions when exposed to low salinity water, the better the oil recovery [37]. Other work suggested that reducing the salinity affects the oil-brine interface viscoelasticity and hence the efficacy of LSW [38,39]. Bartels et al. [40] showed that solid-liquid surface energies play a more significant role in the LSE than fluid-fluid interfacial tension. The observation of water-film expansion in a micromodel experiment emphasized the significance of the solid-liquid interfaces. The development of water films, driven by slow wettability alteration, was simulated by a pore-scale model developed by Akai et al. [41].

Low salinity has been studied mainly on the core and sub-pore scales, with pore-scale studies receiving much less attention [28]. Most pore-scale studies were performed on micro-models where it was not possible to test and study the mechanisms on a natural rock system. Moreover, studies showing direct visualisation and evidence of *in situ* LSW processes in carbonate rocks are rare.

The latest developments in X-ray microtomography (micro-CT) have made it possible to perform pore-scale characterization studies [42,43] with various applications, including enhanced oil recovery and carbon dioxide storage [44,45]. Combining non-invasive imaging with a high-pressure and high-temperature apparatus has provided great insight into *in situ* multiphase flow processes in natural systems [46–48].

X-ray imaging has been previously used to study LSW [49–53], with only a few studies on carbonate rocks [27,54–56]. Using micro-CT imaging, Qin et al. [57] compared high and low salinity flooding at reservoir conditions. Their study investigated the impact of temperature and initial water saturation on wettability alteration. They proposed that the higher recovery from LSW was mainly due to decreased threshold capillary pressure allowing oil displacement from more pores. There were, however, some limitations related to the wettability characterization methods, e.g., few contact angle measurements, imaging only part of the rock sample, and focusing merely on pore occupancy analysis to address the LSE. Understanding the inter-relationship between oil recovery, wettability changes and pore-scale displacement processes and mechanisms remains incomplete.

Selem et al. [27] conducted a pore-scale study to investigate wettability, fluid configuration and oil recovery from secondary LSW. Using contact angle measurements on hundreds of thousands of points in the image and quantification of oil-brine curvatures and fluid occupancy maps revealed a wettability shift towards a mixed-wet state. Moreover, imaging the whole sample captured the redistribution of oil in the pore space. However, only low salinity brine was injected during the waterflood. Here we extend this work to tertiary LSW, where both high and low salinity brines were injected, and build on some previous preliminary results [58] allowing for a comparison of the two LSW modes.

Therefore, the aim of this work is to provide unprecedented insights into high and low salinity waterflooding by combining coreflooding, *in situ* imaging and a suite of image processing and analysis tools to investigate the pore-scale effects of LSW and compare these effects with high salinity waterflooding (HSW). After going through a wettability alteration process, a carbonate rock sample was injected with high and low salinity brines. Waterflooding was performed at increasing flow rates in a capillary-dominated regime. High-resolution images captured the displacement processes during high and low salinity floods. Moreover, the fluid saturation and the wetting state of the system were analysed throughout waterflooding. This study offers a pore-scale visualization of *in situ* displacement process in a heterogeneous carbonate rock sample at subsurface conditions. It highlights the interplay between the observed mechanisms, fluids configuration and wettability changes to understand further how LSW can be employed to enhance oil recovery from carbonate reservoirs.

2. Materials and methods

2.1. Materials

The rock used in this study was a carbonate quarry rock, Estaillades, composed of 97 wt% calcite with traces of dolomite [59,60]. Estaillades has a bimodal pore size distribution, prolific intergranular macro-porosity, and abundant micro-porosity in the bioclasts. A cylindrical rock sample, 6 mm in diameter and 12 mm in length, was used in the coreflooding experiment. The sample had a porosity of 0.293 ± 0.003, measured using a helium porosimeter (AccuPyc II 1340), and an absolute permeability of 0.11 ± 0.03 Darcy calculated from pressure drop measurements during brine injection.

Table 1 shows the composition and salinity of each brine used in this study and the total acid and base numbers and the SARA (Saturates, Aromatics, Resins, Asphaltenes) analysis results for the crude oil. Formation brine (FB), high salinity brine (HSB) and low salinity brine (LSB) were formulated in the lab as synthetic solutions of several pure salts (supplied by Sigma-Aldrich) in deionized water. HSB was prepared as desulphated seawater, and LSB as a more dilute salt solution. The viscosity values, at 70 °C, of HSB and LSB are 0.448 and 0.426 mPa·s, respectively. The oil was dehydrated and filtered to remove any residue or dispersed solid. The interfacial tension (IFT) between oil and, FB and LSB is 16.3 and 22.3 mN/m, respectively, measured at 35 °C.

Table 1
Composition and properties of the fluids used in this study.

	Salt concentration (g/L)						
	NaCl	KCl	$CaCl_2{\cdot}2H_2O$	$MgCl_2{\cdot}6H_2O$	Na_2SO_4	$NaHCO_3$	**Total dissolved solids**
Formation brine (FB)	109.55	0.00	46.070	11.240	0.140	0.200	**167.200**
High salinity brine (HSB)	29.00	0.90	0.605	0.405	0.026	0.156	**31.092**
Low salinity brine (LSB)	0.76	0.035	0.020	0.296	0.087	0.0007	**1.200**

Crude oil

Properties		**SARA analysis**	
Density (kg/m^3) measured at 70 °C	803	Saturates (wt%)	48.40
Viscosity (mPa·s) measured at 70 °C	1.56	Aromatics (wt%)	48.10
Total Acid Number (TAN) (mg KOH/g)	0.34	Resins (wt%)	2.80
Total Base Number (TBN) (mg KOH/g)	0.41	Asphaltenes (wt%)	0.70

2.2. Methods

2.2.1. Experimental apparatus and procedure

The experimental apparatus consisted of a carbon fibre flow cell connected to syringe pumps (Teledyne ISCO) via PEEK tubing and valves to control the pressure and flow rate inside the sample (Fig. 1). The main stages of this experimental study were (i) cleaning and fully saturating the sample with formation brine, (ii) injecting crude oil for 3 weeks, at high temperature, to alter the rock wettability, and (iii) studying the *in situ* effects of changing the injected brine salinity during waterflooding through the acquisition of X-ray images.

The experiment was performed according to the following procedure:

1. A confining pressure of 2 MPa was applied in the isolated space between the Viton sleeve containing the rock sample and the carbon fibre sleeve of the coreholder. The confining pressure squeezed the sleeve onto the sample to avoid fluid side flow.
2. The dry cylindrical sample (called a core) was imaged using a micro-CT scanner.
3. A brine solution made from deionized water with 20 wt% potassium iodide (KI) was injected to characterize the rock bimodal porosity using the differential imaging method [61].
4. The sample was then cleaned by injecting four-times diluted formation brine followed by isopropanol, both for 10 pore volumes. It was dried with a gentle nitrogen flux for 24 h then vacuumed for 3 h.

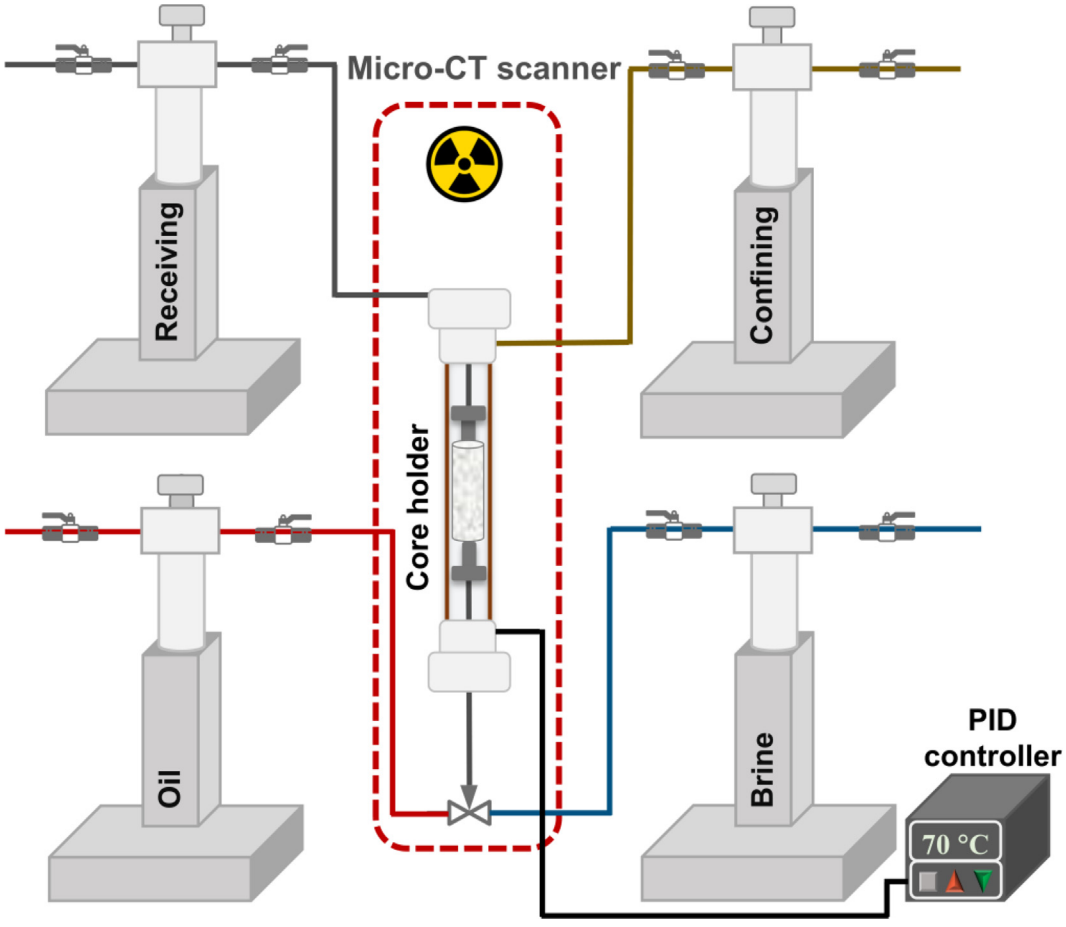

Fig. 1. The experimental apparatus consisting of the flow apparatus and micro-CT scanner used in this study.

5. The formation brine was then injected for 200 pore volumes to saturate the rock sample thoroughly. The sample absolute permeability was measured.
6. Drainage was performed with the injection of viscous synthetic oil at increasing flow rates to reach irreducible water saturation. This synthetic oil has a density and dynamic viscosity of 836 kg/m^3 and 12 mPa·s, respectively, measured at 20 °C.
7. Toluene was injected for 10 PVs to avoid mixing synthetic and crude oils. Crude oil was then introduced at an increased temperature, 50 °C, to avoid wax precipitation.
8. The coreholder assembly was then moved to an oven at 80 °C, and 11 MPa back pressure to change the rock wettability to a similar state found in oil reservoirs (this process is called ageing). Crude oil was injected at a low flow rate (2 μL/min) for three weeks. The flow direction was reversed after 1.5 weeks.
9. After ageing, the temperature in the system was changed to 70 °C using an Omega flexible heating tape and a PID controller, as shown in Fig. 1.
10. Before waterflooding, crude oil mixed with a 20 wt% of 1-iododecane, as a high contrast dopant, replaced the crude oil in the sample to distinguish the oil phase from the brine in the X-ray images to calculate the initial water saturation. The dopant addition increased the IFT between oil and brine by approximately 4 mN/m to 20.3 and 26.3 mN/m for FB and LSB respectively. The value for HSB is similar to that of LSB. The oil asphaltene content remains unchanged when the dopant is used [57].
11. The rock core was flooded with HSB and then LSB, as detailed in the next section.

2.2.2. Waterflooding

The flooding experiment was performed in tertiary mode, i.e., low salinity flooding at the residual oil saturation after high salinity flooding. HSB was injected at a sequence of increasing flow rates; 1, 2, 4, 11, 22 and 42 μL/min at 70 °C. 10 pore volumes were injected at each rate. LSB was then injected following the same procedure. The capillary number was calculated as.

$$Ca = \mu q/\sigma \quad (1)$$

where μ is the viscosity of brine, q is the Darcy velocity of brine, and σ is the oil-brine interfacial tension. The capillary numbers associated with the flow rates indicate capillary force dominated flow conditions with values ranging from approximately 10^{-8} to 10^{-7} at the lowest and highest rates respectively. Table 2 lists the capillary number values for all flow rates. The sample was scanned after the 1, 4, 11 and 42 μL/min injection rates during both the high and low salinity floods. A total of 8 images were acquired throughout waterflooding.

2.2.3. Image acquisition, processing, and segmentation

A micro-CT scanner (HeliScan manufactured by Thermo Fisher) was used to acquire 3D tomograms to study and visualize pore-scale displacement processes and characterize the wetting state of the rock. X-ray images were taken at different points through the experiment: a dry scan before fluid injection (reference image), after ageing and before waterflooding, and during HS and LS waterflooding. Each acquisition took nearly a day, and the size of the acquired images was 2880 × 2880 × 5200 voxels, with a resolution of 2.3 μm/voxel. The images were filtered using non-local means edge-preserving filter to remove image noise [62]. All images were segmented into rock, water and oil phases using a seeded watershed algorithm [63,64]. The segmented images were used to calculate oil and water saturation in the resolved macro-pore space. Since micro-pores are below the image resolution, our analysis focused on macro-pores where the interfaces between oil, brine and rock can be observed for contact angle and curvature measurements.

2.2.4. Characterization of rock wettability and fluid distribution

Contact angles were measured by fitting smoothed surfaces to the oil/brine interfaces, obtained from segmented 3D images, and recording their intersection with the rock surface using defined perpendicular vectors. An automated algorithm was used allowing for hundreds of thousands of contact angle measurements [65]. Curvature measurements were obtained by extracting and smoothing the oil/brine interfaces and determining the principal curvature values and directions using commercial image analysis software, Avizo 9.5 [66–68].

Pore occupancy was determined by applying a generalized pore network extraction algorithm [69,70] to the segmented 3D images with oil and brine labels. This method was used in previous experimental studies [27,71–73]. The occupancy of both pores – wide regions of the void space – and throats – the narrow connections between pores – was quantified. Volume fractions of oil and brine have also been calculated directly from the segmented images to determine the remaining oil saturation after the floods and quantify oil recovery.

3. Results and discussion

Tertiary LSW and the impact of modifying the salinity and composition of injected brine was studied using three-dimensional pore-scale images. We compare the results obtained before waterflooding, and after different high salinity and low salinity waterfloods. In section 3.1, we investigate and visualize displacement processes and mechanisms, such as the formation of water micro-dispersions and the growth of water films, at the pore level because of LSW. In section 3.2, segmented images are used to map fluid occupancy in the pore space. In section 3.3, *in situ* wettability is characterized using interfacial areas, contact angle and curvature measurements as well as calculated capillary pressure. Then, the fluid connectivity using Gaussian curvatures and 3D visualization is demonstrated in section 3.4 followed by a discussion of the interrelationship between this set of results, and the oil saturation and recovery profiles in section 3.5.

3.1. Pore-scale displacement processes and mechanisms

We used the raw images to highlight any variations between the initial case before any waterflooding and the results after both high and low salinity waterflooding. Fig. 2 shows two-dimensional cross-sections of the sample at different stages in the experiment.

Table 2
Waterflooding injection steps with calculated capillary numbers.

Injection rate (μL/min)		**1**	**2**	**4**	**11**	**22**	**42**
Capillary number	**High salinity**	1.02×10^{-8}	2.05×10^{-8}	4.09×10^{-8}	1.13×10^{-7}	2.25×10^{-7}	4.30×10^{-7}
	Low salinity	9.72×10^{-9}	1.94×10^{-8}	3.89×10^{-8}	1.07×10^{-7}	2.14×10^{-7}	4.08×10^{-7}

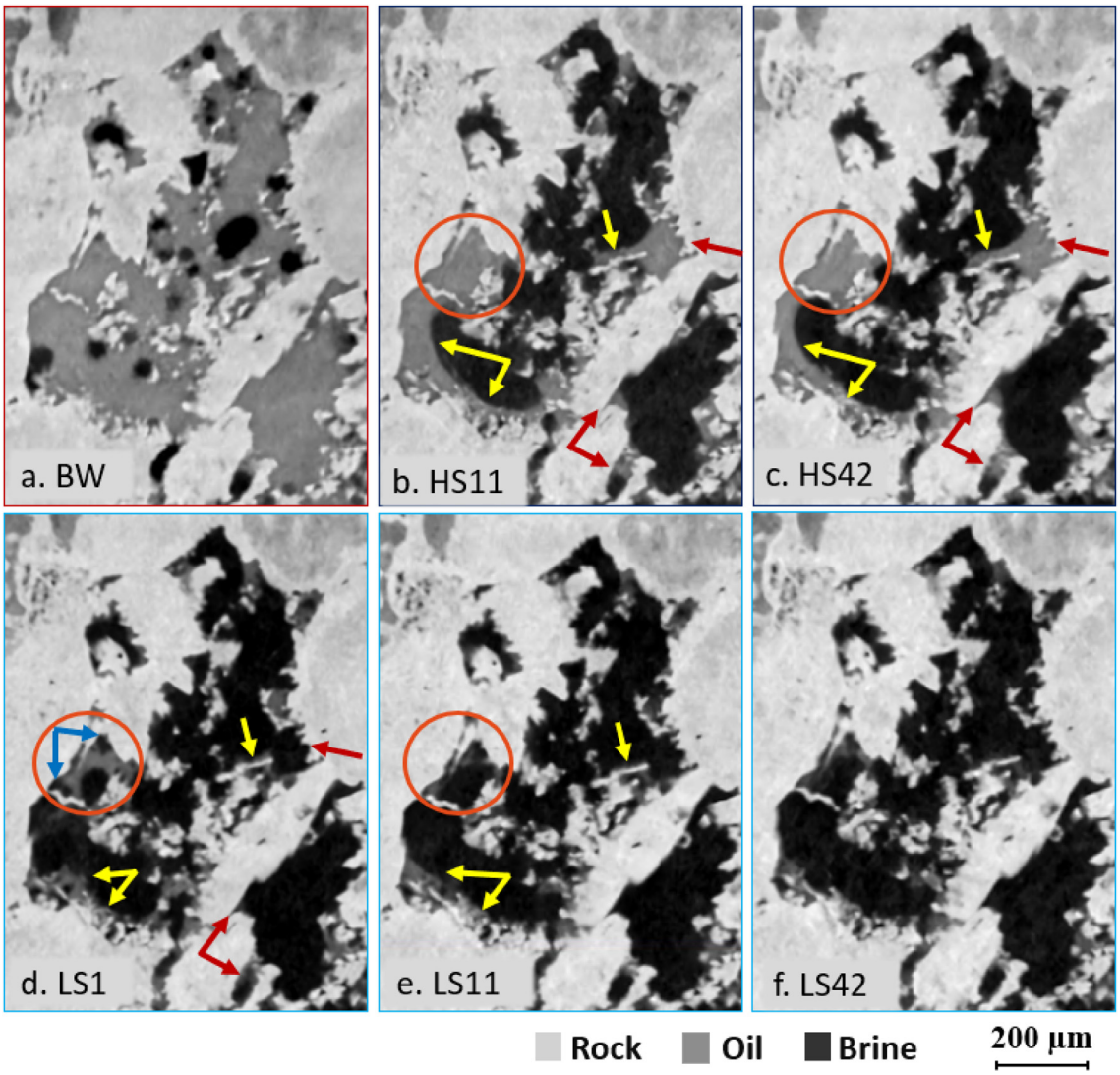

Fig. 2. Two-dimensional cross-sections from the images illustrating the oil and brine distribution in the pores before waterflooding (a), after 11 and 42 µL/min high salinity (HS) floods (b-c), and after the 1, 11 and 42 µL/min LS floods (d-f). The orange circles show immobile oil in a dead-end pore during HSW which was detached from the rock surface by the growth of water droplets (blue arrows) during LSW. The yellow and red arrows highlight the oil constrained to layers and pore corners, respectively, after HSW and the breakup of these layers and displacement of oil from pore corners after LSW.

Initially, oil filled the pore space and brine blobs resided mainly in the centre of the pores (Fig. 2a). With HSW (Fig. 2b-c), the volume of brine increased but oil remained in dead-end pores (orange circles), in pore-corners (red arrows) and layers along the pore walls (yellow arrows). When low salinity brine was injected, significant fluid/fluid and fluid/solid interactions were observed (Fig. 2d-f). The oil layers started to collapse, and oil was displaced from pore corners and dead-end pores. Water domains, highlighted by blue arrows, formed between the oil and the rock surface and, with the continued injection of low salinity brine, they grew displacing most of the oil in the pore, highlighted with orange circles.

In addition to the displacement processes, the images revealed the mechanisms by which oil was displaced during LSW. To investigate these underlying mechanisms further, we had a closer look at individual pores. Fig. 3 shows different pores within which oil was displaced by two main mechanisms during LSW. From an initially oil filled pore, high salinity brine only displaced oil from the pore centres and, despite injecting 60 pore volumes at increasing flow rates, oil remained attached to pore walls and corners (Fig. 3-a-b). However, when LSW started (Fig. 3c), brine appeared between the oil and rock surface (blue circles) and the oil in the top pore was mobilised (blue arrows) to the bottom pore, and after 2 days with LSB injection at higher flow rates a thin water film (blue arch) started to grow and detach the oil from the rock surface (Fig. 3d-e). Oil was also displaced by another mechanism; the development of water micro-droplets (micro-dispersions). After flooding the sample with high salinity brine for 6 days, no significant change was observed from the initial case (Fig. 3f-g). During LSW, water micro-droplets started to form both within the oil phase and at the oil/solid interfaces (Fig. 3h). After two days and more pore volumes of brine injected these droplets grew and coalesced displacing more oil (Fig. 3i). After a few more days, there was a slight increase in the water volume and a change in the contact angle between the oil/brine interfaces and the rock (Fig. 3j) suggesting a change in the wetting conditions. Wettability characterization will be discussed further in section 3.3.

To have a deeper understanding of the role of micro-dispersions in the displacement process, a 3D visualization, extracted from the segmented images, highlights the appearance of these droplets during HSW and their growth as the brine salinity and composition was changed during LSW. The pores were fully occupied by oil before waterflooding (Fig. 4a). Water micro-droplets did not ini-

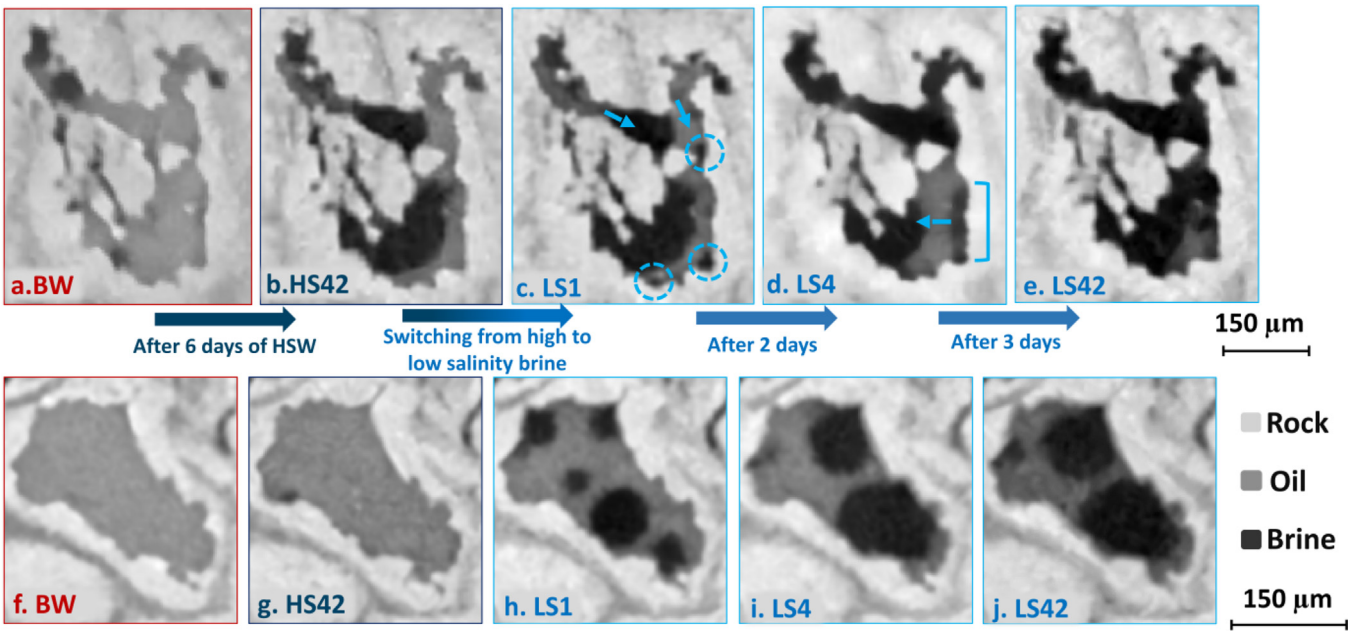

Fig. 3. Two-dimensional cross-sections from the X-ray images highlighting the mechanisms by which oil is displaced during low salinity waterflooding. (a-e) Oil was displaced from the centre of the pore with HSW. Water appeared at the oil/rock interface after LS1, blue circles, and connected to form a layer detaching the oil after LS4, blue arch. (f-j) Water micro-droplets only started to appear and grow after LSW.

tially form during HSW (Fig. 4b) but after the injection of 30 PVs of HSB, some droplets started to appear (Fig. 4c). Brine invaded the centre of the two pores at the top while some residual oil was observed in the pore corners. At the end of HSW (Fig. 4d), and the injection of 60 PVs, a few more droplets formed within the oil phase, while oil remained trapped in pore corners (red arrows). The water droplets grew after the first LS flood (Fig. 4e) and coalesced resulting in volume displacement of oil at the end of LSW (Fig. 4f). Moreover, the trapped oil was mobilized.

There could be a connection between the pore-scale displacement processes and mechanisms observed during waterflooding and the properties of the crude oil-brine-rock (COBR) system used in this study. The acidity and the asphaltene content of the crude, the salinity gradient between FB and HSB, as well as the reduced salinity and increased sulphate concentration of the LSB, compared to HSB, are elements that induced the formation and growth of water micro-dispersions within the oil and at the oil-brine interfaces [29,31,37]. In a secondary LSW experiment, where LSB was injected at initial water saturation into a similar COBR system, the aforementioned mechanisms were rarely observed [27]. This can be explained by the large osmotic gradient between the initial (formation) water and low salinity water which likely increases the rate at which micro-droplets develop and coalesce making the process too fast to be captured by X-ray imaging.

3.2. Pore occupancy mapping

To further understand the configuration of oil and brine across the sample with high and low salinity waterflooding, 3D quantification of pore occupancy was performed. The pore radii are mainly between 10 and 60 µm (Fig. 5a), and throats radii are mainly between 5 and 35 µm (Fig. 5b). Initially, oil occupied most of the pore space with brine residing mainly in larger pores (Fig. 5c) and throats (Fig. 5i). This fluid distribution signifies oil-wet conditions [27,74,75]. After HSW, brine displaced oil from relatively larger pores (pore radius > 10 µm), but oil still occupied most of the smaller pores and throats. Additional oil was only displaced when the flow rate was increased, indicating that large regions of the pore space remained oil wet during HSW. This is shown in Fig. 5-d-e for pores and Fig. 5j-k for throats. During LSW, more oil was displaced from smaller pores (Fig. 5f-h), which is in line with observations made in section 3.1. The fraction of throats occupied by oil decreased slightly after LSW (Fig. 5l-n). The brine filling of smaller pores after switching to LSW, even when injected at a low flow rate, can be explained by the mechanisms discussed in the previous section and is characteristic of the low salinity effect and wettability changes. In the secondary LSW study, similar initially oil-wet conditions were detected; however, through LSW, a redistribution of oil from smaller to larger pores was observed which facilitated the recovery of oil as more brine was injected [27]. This rearrangement was not observed in the tertiary mode and could be the underlying reason for the difference in recovery factors between the two modes as will be discussed later.

The pore-scale displacement processes and mechanisms observed after LSW, namely the collapse of oil layers, formation of water micro-dispersions and the displacement of oil from pore corners and small pores, could be related to the change in the wettability of the rock from oil-wet conditions before and during HSW towards mixed-wet conditions after LSW.

In the next section, we assess the magnitude of wettability alteration after HSW and LSW by the analysis of interfacial areas, contact angles and curvatures. We will also examine whether there is a relationship between the wettability and the mechanisms discussed hitherto.

3.3. Wettability characterization

The fluid occupancy maps give an indication of the fluid distribution in the pore space, but they only show which fluid occupies the largest fraction of the pore and do not capture the fluids residing in the pore corners or as layers along the pore walls. Therefore, to complement the pore occupancy analysis, we calculated the interfacial area per unit volume between oil-water, water-solid and oil-solid. The measurements of interfacial area per unit volume

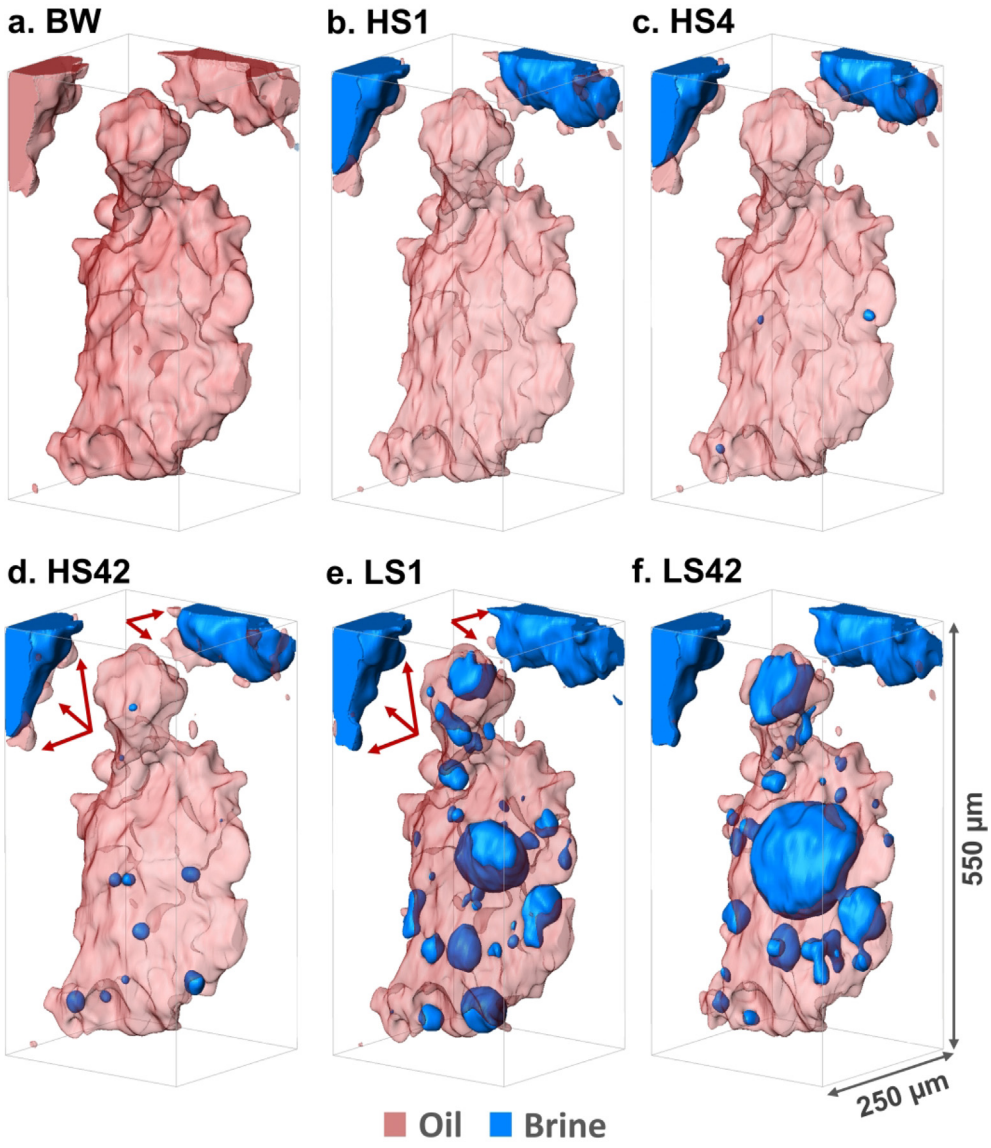

Fig. 4. A three-dimensional visualization of oil-filled pores before waterflooding (a), and the development of water micro-droplets during HSW (b-d) and their growth during LSW (e-f). The red arrows highlight the displacement of oil trapped in pore corners by the low salinity brine injection. The brine, oil and rock are shown as blue, semi-transparent red and transparent, respectively.

in resolved pores are shown in Fig. 6a. To remove the voxelization artefacts associated with the segmented images, the interfaces were smoothed using Gaussian smoothing [76]. The oil-solid interfacial area decreased to a value equal to that of the water-solid interfacial area towards the end of HSW, while the oil-water interfacial area increased to a maximum value. This can be explained, as discussed in section 3.1, by oil layers covering the oil-wet rock surfaces [77]. After LSW, a drop in both the oil-solid and oil-water interfacial areas is observed. This is due to the breakdown of the oil layers, formation of water micro-droplets, and the displacement of oil from pore corners and dead-end pores allowing the brine to directly contact the rock surface resulting in a change in wettability and further mobilization of oil.

To further evaluate the effect of high and low salinity water injection on wettability with the change in flow rate, contact angles and curvatures were measured using oil-brine interfaces. The spatial distribution of contact angles on the contact line between oil, water and rock was used to assess the wettability [63,78]. *In situ* contact angle and curvature measurements histograms showed a shift after HSW and LSW. Initially, the mean contact angle was 115° ± 18° which changed only slightly to 112° ± 20° at the end of HSW showing the oil-wet nature of the sample. After the LSW, a substantial shift occurred with a mean contact angle of 102° ± 15° (Fig. 6b).

In addition to calculating interfacial areas, the oil-water interfaces were used to estimate curvatures which can reveal details about rock wettability, local capillary pressures, and fluid connectivity. The smoothed oil-water interfaces were used to extract the two principal curvatures (κ_1 and κ_2), from which the mean curvature κ is calculated as an average. Before waterflooding, and during HSW the mean curvature values are negative (Fig. 6c). The negative curvature values can also be explained by the morphology of the fluid interfaces in Fig. 3a-c where brine bulged into oil indicating an oil-wet system. With LSW, the fraction of the positive curvatures increase explaining the shift in the mean curvatures values.

The changes in the contact angles and mean curvature values after switching from high to low salinity brine suggest that the rock surfaces display a shift from the initial oil-wet conditions towards more mixed-wet conditions.

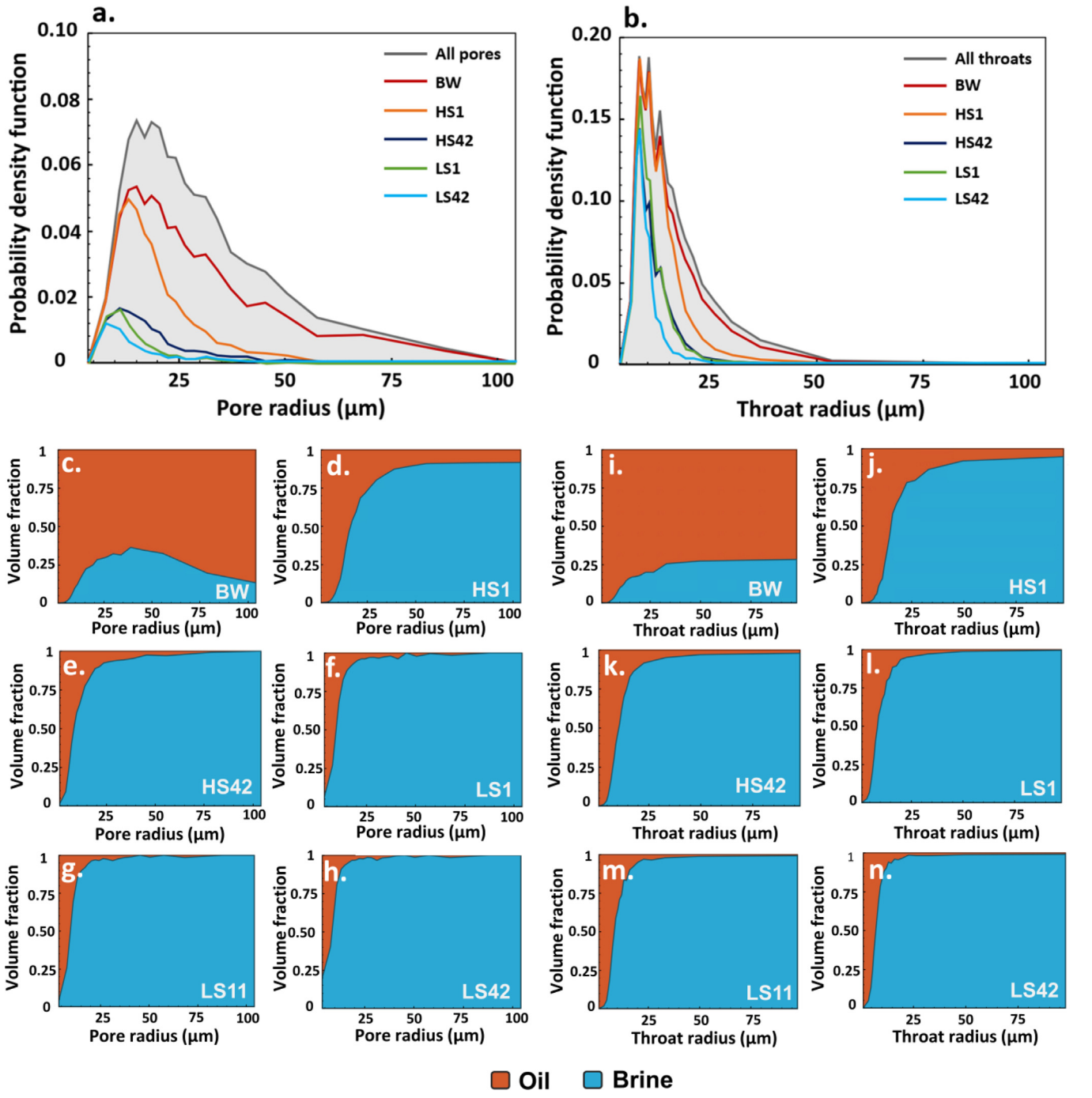

Fig. 5. Histogram plots showing the size distribution of resolved pores (a) and throats (b) and the volume-weighted fraction of oil-filled pores and throats computed using the generalized pore network extraction tool at different stages of waterflooding. (c-n) Fluid occupancy maps for pores and throats of different radii before waterflooding and for HS and LS waterflooding.

The local capillary pressure was calculated using the Young-Laplace law:

$$P_c = 2\sigma\kappa \tag{2}$$

where σ is the oil-water interfacial tension and κ is the average curvature of the interface between oil and water. The mean curvature values were used to calculate the capillary pressure of the system [66,77,79] before waterflooding and after various injection steps (Fig. 6d). Negative capillary pressure values before waterflooding and through HSW, are reflective of oil-wet conditions. However, after LSW, the values showed a change towards increased water-wetness. With an increase in capillary pressure, brine can invade and displace oil from smaller pores. The wettability change is more significant than the normal trend of capillary pressure, namely a decrease with increasing water saturation, seen when the wettability remains constant throughout the displacement.

3.4. Fluid connectivity

Curvature measurements were also used to evaluate fluid connectivity from the product of the two principal curvatures (κ_1 and κ_2), defined as the Gaussian curvature [80,81]. It has a negative

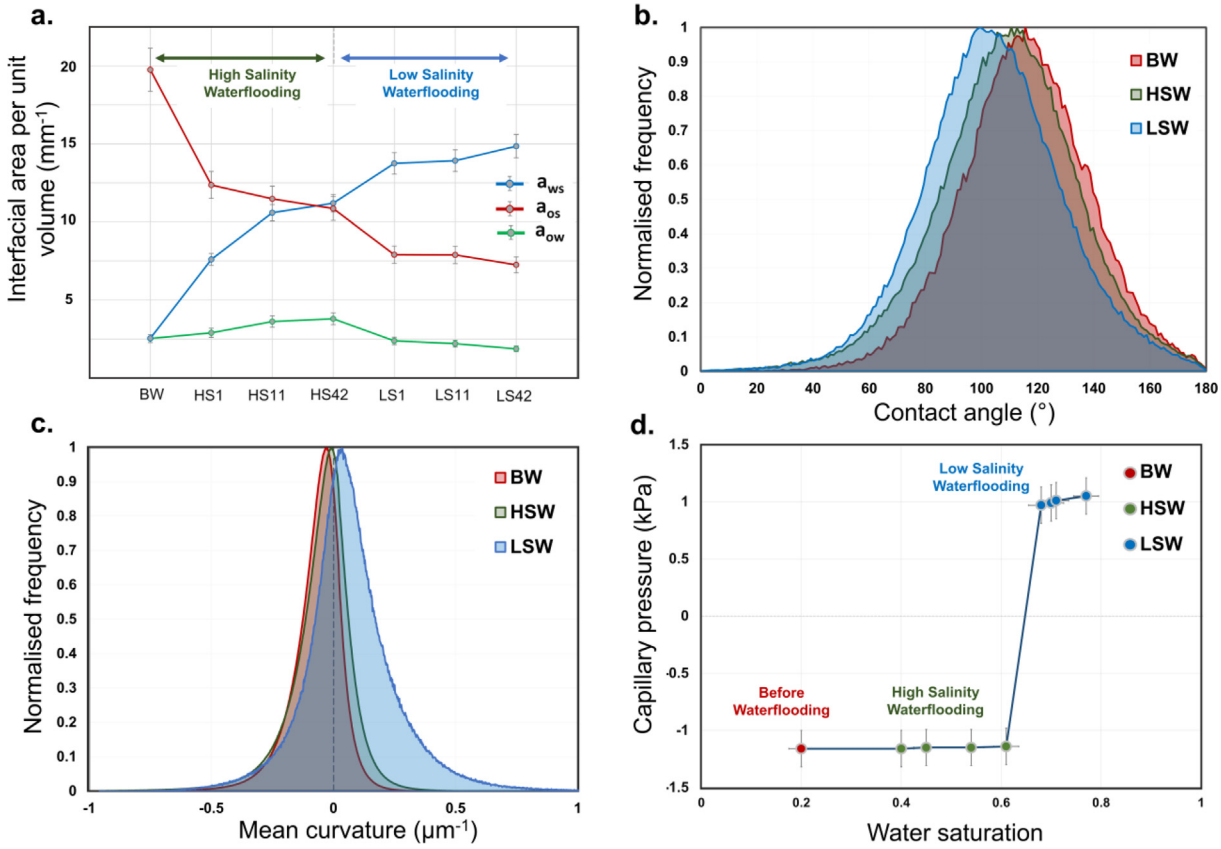

Fig. 6. (a) Oil-water, water-solid and oil-solid interfacial areas per unit volume: a_{ow}, a_{ws} and a_{os} respectively. Histograms of contact angle distributions (b) and mean curvatures (c) measured from the segmented 3D images. (d) Capillary pressure values calculated from the mean oil/brine interfacial curvatures before waterflooding (BW) and after different steps of high and low salinity waterflooding. The error bars indicate the uncertainty in the segmentation and the measurements of curvature and saturation.

value for well-connected phases and the opposite if the phases are poorly connected. To better understand the phase connectivity in the system, principal curvatures were categorized into three groupings: both positive ($\kappa_1 > 0$, $\kappa_2 > 0$), both negative ($\kappa_1 < 0$, $\kappa_2 < 0$), and of opposite signs ($\kappa_1\ \kappa_2 \leq 0$). Initially, the curvature distributions show predominantly negative principal curvatures, i.e., positive Gaussian curvature, indicating a lack of connection of the water phase within the pore space (Fig. 7a). A similar distribution is shown after HSW (Fig. 7b) where, despite the increase in water saturation, the oil phase remains better connected through oil layers, as discussed in sections 3.1 and 3.2, indicative of the oil-wet state of the system [79]. After LSW, most of the curvatures have one positive and one negative value, i.e., a negative Gaussian curvature, Fig. 7c-d. The increase in interfaces with two positive principal curvatures (the blue histogram) corresponds, unlike in HSW, to poorly connected oil in water-wet regions. This indicates a mixed-wet, or weakly water-wet, system with reasonable connectivity of both phases in the pore space [72,77,79].

To further understand the fluid connectivity, Fig. 8 shows how different brine ganglia in one part of the rock sample became connected during waterflooding. Initially, water clusters were dispersed and occupied the centre of the pores (Fig. 8a). During HSW, water micro-droplets started to develop, albeit slowly (Fig. 8-b-d). As LSW started, water micro-droplets grew and connected forming continuous water layers (Fig. 8e-f). The development of the blue brine blob, in the top right corner, highlights this process. The pore encircled in red was fully oil-saturated before waterflooding and after the first HS flood (Fig. 8a-b). Water micro-dispersions started to form only after 3 days, and 30 pore volumes, of HSB injection (Fig. 8c). Injecting more HSB did not result in a significant difference (Fig. 8d). However, switching to LSB triggered the growth of water micro-dispersions and a substantial increase in their size was observed (Fig. 8e-f). For example, the volume of the main brine ganglion in Fig. 8, shown in blue, has increased by four times after 60 PVs of HSB injection. After the first LS flood, 10 PVs of LSB injection at 1 μL/min, the ganglion size further increased by more than seven times, and the injection of more LSB resulted in a small volume increase. The ganglion volume increased due to the growth of the ganglion itself and by the coalescence with nearby droplets resulting in the displacement of oil as discussed in section 3.1.

3.5. Oil saturation and recovery profiles

The initial water saturation, before waterflooding, was calculated from the segmented 3D image as 11%. The saturation profiles of oil across the sample at different stages are shown in Fig. 9a. The oil saturation decreased with time during the HSW, especially after the highest flow rate injection (HS42), indicating an oil-wet sample [82]. Oil was displaced by the invasion of HSB to the centre of pore space, as discussed in sections 3.1 and 3.2. By the end of HSW, 57% of the original oil in place (OOIP) in resolved pores was recovered, as shown in Fig. 9b. With LSW, more oil was recovered. After 10 pore volumes (PVs) of LSB were injected at 0.001 mL/min, an additional 3% of oil was recovered. By the end of LSW, the ultimate recovery reached 66%, i.e., LSW resulted in an incremental oil recovery of 9%.

The low salinity effect was not instant; there was first a rearrangement of detached oil in the pore space before it was displaced towards the outlet. Two phenomena were observed that led to oil

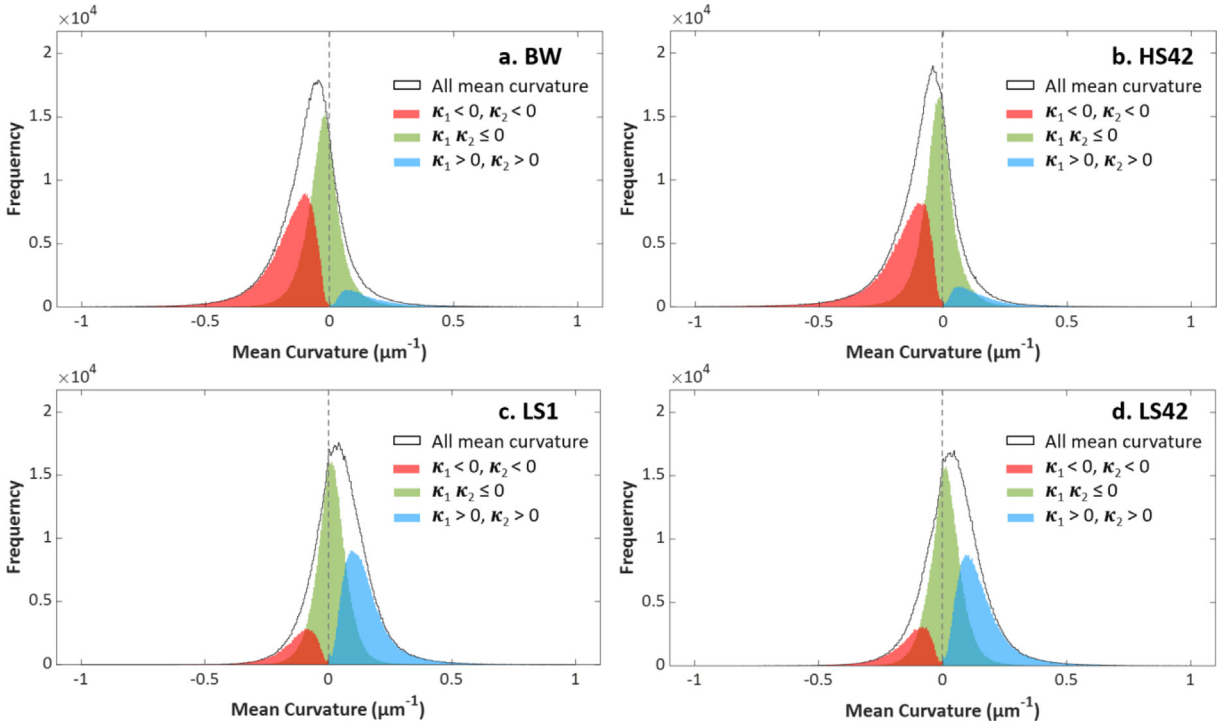

Fig. 7. Measured oil-brine curvature distribution (a) before waterflooding (BW), (b) after the last high salinity flood (HS42), (c) after the first low salinity flood (LS1), and (d) after the last low salinity flood (LS42) using the principal curvatures (κ_1 and κ_2) extracted from smoothed oil-water interfaces. The black curve shows the mean curvature distribution. The red, green, and blue histograms show the distributions of κ_1 and κ_2 values that are both negative, of opposite signs, and both positive respectively.

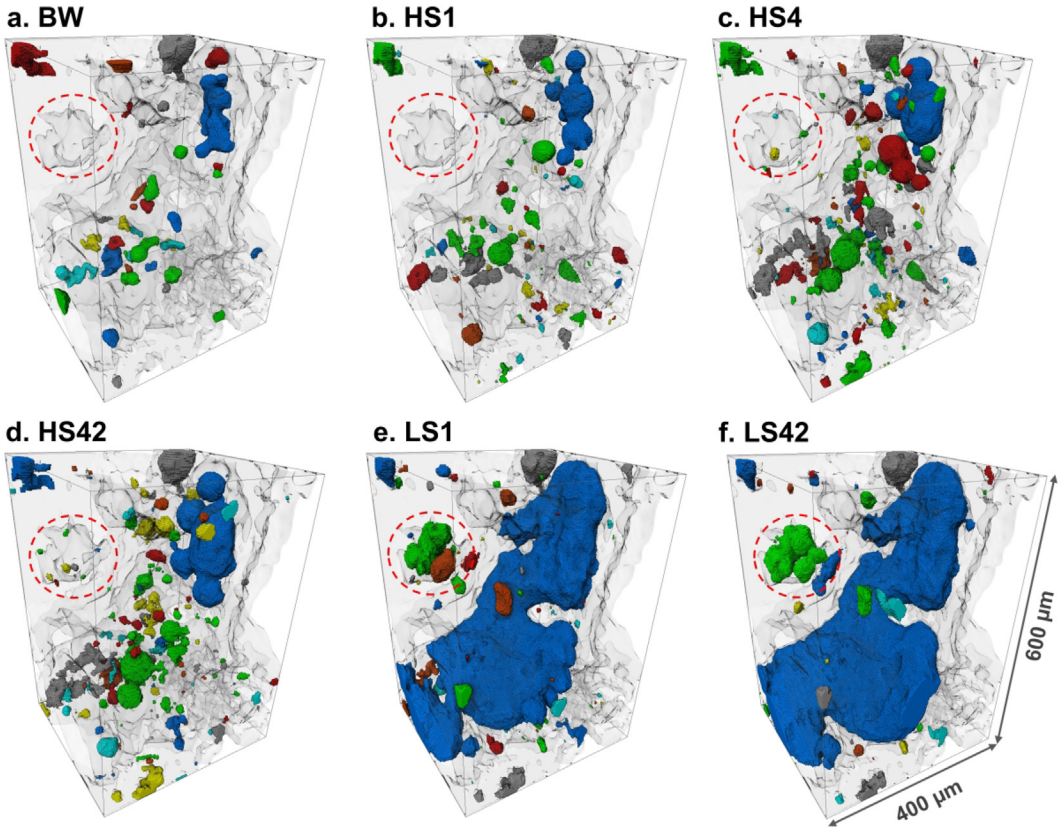

Fig. 8. Three-dimensional visualizations of the development and connection of water domains before waterflooding (a) after HS floods (b-d) and LS floods (e-f). Different colours represent different connected brine blobs. Oil is transparent and rock is semi-transparent. The volume, in 10^6 μm^3, of the largest brine ganglion, highlighted in blue, at the different stages is 0.34, 0.48, 0.86, 1.37, 10.7 and 11.32, respectively. The red circles show the slow formation of water micro-droplets during HSW and the fast rate at which they developed and coalesced during LSW.

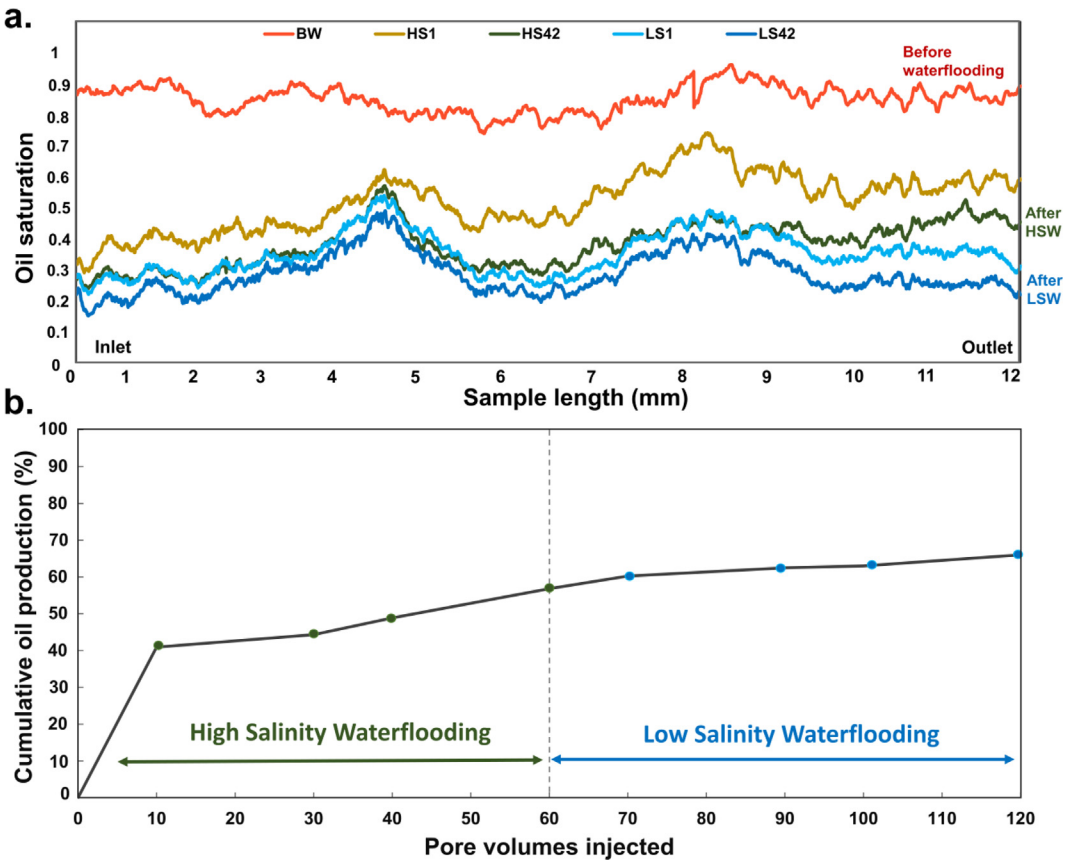

Fig. 9. (a) Oil saturation profiles across the sample before waterflooding (BW) and at different stages of HSW and LSW. (b) The cumulative oil recovery at different points of waterflooding.

detachment and mobilization: the formation of water micro-droplets within the oil phase and at the oil/solid interfaces, and then the merging of water domains forming thin water films. Fig. 3a indicates that the expansion of the water film detaching the oil followed by the reconnection of the oil ganglia occurred after 2–3 days of LSB injection.

We propose that the possible formation of water micro-dispersions in oil caused oil swelling, i.e., the increase in oil volume which resulted in the reconnection of oil enhancing the oil mobility and ultimately increasing oil recovery factor.

4. Conclusions

In this study, we used X-ray imaging to observe the *in situ* development of low salinity mechanisms on a natural system and characterized the associated changes in rock wettability as well as the impact on oil recovery. We studied tertiary LSW in a carbonate rock sample.

For our combination of crude oil, brine and rock, a response to LSW was demonstrated. The distribution of the oil phase, before and during the HS floods, in dead-end regions of the pore space and expanding along the pore walls is indicative of the relatively strong propensity of the rock surface to oil, consistent with the measured high contact angle and negative capillary pressure values. After LSW, the development of water micro-droplets at the oil/brine and oil/rock interfaces and in the oil phase, as well as the expansion of thin water films between the oil and rock surface were observed. Water film swelling and micro-dispersions are considered the underlying mechanisms for the wettability alteration and ultimately the low salinity effect observed in this study. This is in line with observations from previous studies on the relationship between water-in-oil micro-dispersions and crude oil properties [31,32,83]. The formation of micro-dispersions, driven by diffusion and osmosis, resulted in oil displacement and mobilization [33,35].

Unlike in previous work [31], our results show a gradual formation of water micro-dispersions during HSW, which is due to the salinity difference between FB, or irreducible water, and HSB until osmotic equilibrium is reached. It was also observed that, after switching to LSW, oil in the pores in which micro-droplets had formed during HSW, was recovered faster than in the pores that remained intact after HSW. The fast coalescence of water micro-droplets during LSW is driven by the significant differences in salinity, and ionic strength, between the LSB and the brine in the system. This explains the inability to capture the development of water micro-droplets during secondary LSW [27].

Analyses of contact angles, curvatures, capillary pressures, and pore occupancy indicated a shift in the rock wettability from oil-wet towards mixed-wet conditions due to LSW. The change in wettability, induced by LSW, improved the microscopic sweep efficiency as the result of increased capillary forces [27]. The underlying mechanisms and subsequent change in wettability resulted in a 9% increase in oil recovery. A similar increase in recovery was obtained in a previous tertiary LSW coreflooding experiment [82]. The results from our previous experimental study showed that, when compared to tertiary LSW, secondary LSW is more efficient and achieved a higher recovery factor [27]. When injecting LSB in secondary mode 85% of the oil, in the pore space resolved by X-ray imaging, was recovered compared to 66% in tertiary mode. In tertiary mode, the local displacement efficiency is lower, as the brine continues to follow principally the flow path-

ways established during the initial, inefficient, high salinity flood. Moreover, the rate of micro-dispersions formation during secondary LSW was faster, compared to tertiary LSW, which enhanced oil mobilization and displacement.

This comprehensive LSW study provides insights into the pore-scale displacement mechanisms previously observed only on micro-models [26,31,35]. These results can help interpret the outcome from Darcy and molecular scale experiments, hence bridging the gap between these very different length scales. Moreover, this study can deliver valuable input for the brine selection criteria to design LSW-EOR. Finally, the quantitative experimental measurements presented can be used for pore-scale modelling validation and upscaling in enhanced oil recovery projects.

In ongoing studies, a different system of crude oil, brine and reservoir rock is being tested. Future work could focus on understanding the dynamics of water micro-dispersions and thin water films development and the time response of LSW.

CRediT authorship contribution statement

Ahmed M. Selem: Conceptualization, Data curation, Formal analysis, Investigation, Methodology, Validation, Visualization, Writing – original draft. **Nicolas Agenet:** Conceptualization, Investigation, Validation. **Martin J. Blunt:** Conceptualization, Investigation, Supervision, Validation, Writing – review & editing. **Branko Bijeljic:** Conceptualization, Investigation, Methodology, Supervision, Validation, Writing – review & editing.

Declaration of Competing Interest

The authors declare that they have no known competing financial interests or personal relationships that could have appeared to influence the work reported in this paper.

Acknowledgements

We gratefully acknowledge TotalEnergies for funding and providing the material for this study. We would like to thank Ali Raeini for his help with pore-network extraction and fluid occupancy mapping. We also would like to thank our colleagues at TotalEnergies for technical discussions. We would like to thank Alexandra Klimenko for reviewing the manuscript. Branko Bijeljic is also very grateful to TotalEnergies for funding his Senior Fellowship.

References

[1] M. Akbar, B. Vissapragada, A.H. Alghamdi, D. Allen, M. Herron, A. Carnegie, et al., A snapshot of carbonate reservoir evaluation, Oilfield Rev. 12 (4) (2000) 20–21.
[2] F.F. Craig, The reservoir engineering aspects of water flooding, Henry L. Doherty Memorial Fund of AIME, New York, 1971.
[3] H. Mahani, T. Sorop, D.J. Ligthelm, D. Brooks, P. Vledder, F. Mozahem, et al. Analysis of field responses to low-salinity waterflooding in secondary and tertiary mode in Syria, in: SPE Europec/EAGE Annual Conference and Exhibition. 2011. SPE-142960-MS.
[4] N. Morrow, J. Buckley, Improved Oil Recovery by Low-Salinity Waterflooding. JPT. 63 (05) (2011) 106-112. SPE-190230-MS.
[5] P.C. Smalley, A.H. Muggeridge, M. Dalland, O.S. Helvig, E.J. Høgnesen, M. Hetland, et al., Screening for EOR and Estimating Potential Incremental Oil Recovery on the Norwegian Continental Shelf, SPE Improved Oil Recovery Conference. 2018.
[6] P.P. Jadhunandan, N.R. Morrow, Effect of Wettability on Waterflood Recovery for Crude-Oil/Brine/Rock Systems, SPE Res Eng.10(01) (1995) 40-6. SPE-22597-PA.
[7] G.Q. Tang, N.R. Morrow, Salinity, Temperature, Oil Composition, and Oil Recovery by Waterflooding, SPE-36680-PA 12(04) (1997) 269-76.
[8] N.R. Morrow, G.-Q. Tang, M. Valat, X. Xie, Prospects of improved oil recovery related to wettability and brine composition, J. Petrol. Sci. Eng. 20 (3–4) (1998) 267–276.
[9] P. Vledder, I.E. Gonzalez, J.C. Carrera Fonseca, T. Wells, D.J. Ligthelm, Low Salinity Water Flooding: Proof Of Wettability Alteration On A Field Wide Scale, SPE Improved Oil Recovery Symposium; Tulsa, Oklahoma, USA, April 2010. SPE-129564-MS.
[10] M. Kumar, A. Fogden, N.R. Morrow, J.S. Buckley, Mechanisms of Improved Oil Recovery From Sandstone by Low Salinity Flooding, Petrophysics - The SPWLA J. Form. Eval. Reserv. Descr. 52 (06) (2011) 428–436.
[11] H. Mahani, S. Berg, D. Ilic, W.-B.-B. Bartels, V. Joekar-Niasar, Kinetics of Low-Salinity-Flooding Effects, SPE J, 20 (01) (2014) 8-20. SPE-165255-PA.
[12] S.-A. Abdolmohsen, A.M. Abdalla, S.I. Mohd, V.P.P. Jose, Experimental investigation into effects of crude oil acid and base number on wettability alteration by using different low salinity water in sandstone rock, J. Jpn. Pet. Inst. 58 (4) (2015) 228–236.
[13] S. Strand, E.J. Høgnesen, T. Austad, Wettability alteration of carbonates—Effects of potential determining ions (Ca2+ and SO42−) and temperature, Colloids Surf., A 275 (1) (2006) 1–10.
[14] P. Zhang, T. Austad, Wettability and oil recovery from carbonates: Effects of temperature and potential determining ions, Colloids Surf. APhysicochem. Eng. Aspects. 279 (1) (2006) 179–187.
[15] S.J. Fathi, T. Austad, S. Strand, "Smart Water" as a Wettability Modifier in Chalk: The Effect of Salinity and Ionic Composition, Energy Fuels 24 (4) (2010) 2514–2519.
[16] A.A. Yousef, S.H. Al-Saleh, A. Al-Kaabi, M.S. Al-Jawfi, Laboratory Investigation of the Impact of Injection-Water Salinity and Ionic Content on Oil Recovery From Carbonate Reservoirs. SPE Reservoir Evaluation and Engineering 14 (05) (2011) 578-593. SPE-137634-PA.
[17] H.H. Al-Attar, M.Y. Mahmoud, A.Y. Zekri, R. Almehaideb, M. Ghannam, Low-salinity flooding in a selected carbonate reservoir: experimental approach, J. Pet. Explor. Prod. Technol. 3 (2) (2013) 139–149.
[18] M.D. Jackson, D. Al-Mahrouqi, J. Vinogradov, Zeta potential in oil-water-carbonate systems and its impact on oil recovery during controlled salinity water-flooding, Sci. Rep. 6 (2016) 37363.
[19] S. Li, M.D. Jackson, N. Agenet, Role of the calcite-water interface in wettability alteration during low salinity waterflooding, Fuel 276 (2020) 118097.
[20] A.A. Yousef, S. Al-Saleh, M. Al-Jawfi, Improved/Enhanced Oil Recovery from Carbonate Reservoirs by Tuning Injection Water Salinity and Ionic Content, SPE Improved Oil Recovery Symposium. Tulsa, OK, April 14−18, 2012. SPE-154076-MS.
[21] J.C. Seccombe, A. Lager, K.J. Webb, G. Jerauld, E. Fueg, Improving Wateflood Recovery: LoSalTM EOR Field Evaluation. SPE/DOE Symposium on Improved Oil Recovery, Tulsa, OK, 20–23 April 2008. SPE-113480-MS.
[22] A.A. Yousef, J. Liu, G. Blanchard, S. Al-Saleh, T. Al-Zahrani, R. Al-Zahrani, et al., SmartWater Flooding: Industry's First Field Test in Carbonate Reservoirs, SPE Annual Technical Conference and Exhibition, San Antonio, Texas, 8–10 October 2012. SPE-159526-MS.
[23] G.-Q. Tang, N.R. Morrow, Influence of brine composition and fines migration on crude oil/brine/rock interactions and oil recovery, J. Petrol. Sci. Eng. 24 (2) (1999) 99–111.
[24] P.L. McGuire, J.R. Chatham, F.K. Paskvan, D.M. Sommer, F.H. Carini, Low Salinity Oil Recovery: An Exciting New EOR Opportunity for Alaska's North Slope, SPE Western Regional Meeting, Irvine, California, USA, 30 March–1 April (2005). SPE-93903-MS.
[25] H. Mahani, A.L. Keya, S. Berg, W.-B. Bartels, R. Nasralla, W.R. Rossen, Insights into the Mechanism of Wettability Alteration by Low-Salinity Flooding (LSF) in Carbonates, Energy Fuels 29 (3) (2015) 1352–1367.
[26] M. Sohrabi, P. Mahzari, S.A. Farzaneh, J.R. Mills, P. Tsolis, S. Ireland, Novel Insights Into Mechanisms of Oil Recovery by Use of Low-Salinity-Water Injection, SPE J, 2017;22(02):407-16. SPE-1072778-PA.
[27] A.M. Selem, N. Agenet, Y. Gao, A.Q. Raeini, M.J. Blunt, B. Bijeljic, Pore-scale imaging and analysis of low salinity waterflooding in a heterogeneous carbonate rock at reservoir conditions, Sci. Rep. 11 (1) (2021) 15063.
[28] W.B. Bartels, H. Mahani, S. Berg, S.M. Hassanizadeh, Literature review of low salinity waterflooding from a length and time scale perspective, Fuel 236 (2019) 338–353.
[29] K.H. Chakravarty, P.L. Fosbøl, Thomsen K. Brine Crude Oil Interactions at the Oil-Water Interface, in: SPE Asia Pacific Enhanced Oil Recovery Conference; Kuala Lumpur, Malaysia, August 2015. SPE-174685-MS.
[30] B. Wei, R. Wu, L. Lu, X. Ning, X. Xu, C. Wood, et al., Influence of Individual Ions on Oil/Brine/Rock Interfacial Interactions and Oil-Water Flow Behaviors in Porous Media, Energy Fuels 31 (11) (2017) 12035–12045.
[31] A. Emadi, M. Sohrabi, Visual Investigation of Oil Recovery by Low Salinity Water Injection: Formation of Water Micro-Dispersions and Wettability Alteration, SPE Annual Technical Conference and Exhibition, New Orleans, 30 September–2 October 2013. SPE-166435-MS.
[32] P. Mahzari, M. Sohrabi, Crude Oil/Brine Interactions and Spontaneous Formation of Micro-Dispersions in Low Salinity Water Injection, SPE Improved Oil Recovery Symposium; 2014. SPE-169081-MS.
[33] K. Sandengen, A. Kristoffersen, K. Melhuus, L.O. Jøsang, Osmosis as Mechanism for Low-Salinity Enhanced Oil Recovery, SPE J, 2016;21(04):1227-35. SPE-179741-PA.
[34] M. AlHammadi, P. Mahzari, M. Sohrabi, Fundamental investigation of underlying mechanisms behind improved oil recovery by low salinity water injection in carbonate rocks, Fuel 220 (2018) 345–357.

[35] S.B. Fredriksen, A.U. Rognmo, M.A. Fernø, Pore-scale mechanisms during low salinity waterflooding: Oil mobilization by diffusion and osmosis, J. Petrol. Sci. Eng. 163 (2018) 650–660.
[36] J. Dubouć, M. Bourrel, E.S. Carreras, A. Klimenko, N. Agenet, N. Passade-Boupat, et al., Auto-Emulsification of Water at the Crude Oil/Water Interface: A Mechanism Driven by Osmotic Gradient, Energy Fuels 33 (8) (2019) 7020–7027.
[37] P. Mahzari, M. Sohrabi, J.M. Façanha, The Decisive Role of Microdispersion Formation in Improved Oil Recovery by Low-Salinity-Water Injection in Sandstone Formations, SPE J, 2019;24(06):2859-73. SPE-197067-PA.
[38] T.E. Chávez-Miyauch, Y. Lu, A. Firoozabadi, Low salinity water injection in Berea sandstone: Effect of wettability, interface elasticity, and acid and base functionalities, Fuel 263 (2020) 116572.
[39] T. Kar, H. Cho, A. Firoozabadi, Assessment of low salinity waterflooding in carbonate cores: Interfacial viscoelasticity and tuning process efficiency by use of non-ionic surfactant, J. Colloid Interface Sci. 607 (2022) 125–133.
[40] Bartels W-B-B, Mahani H, Berg S, Menezes R, van der Hoeven JA, Fadili A. Oil Configuration Under High-Salinity and Low-Salinity Conditions at Pore Scale: A Parametric Investigation by Use of a Single-Channel Micromodel. SPE J, 2017;22(05):1362-73. SPE-181386-PA.
[41] T. Akai, M.J. Blunt, B. Bijeljic, Pore-scale numerical simulation of low salinity water flooding using the lattice Boltzmann method, J. Colloid Interface Sci. 566 (2020) 444–453.
[42] C.H. Arns, F. Bauget, A. Limaye, A. Sakellariou, T. Senden, A. Sheppard, et al., Pore Scale Characterization of Carbonates Using X-Ray Microtomography, SPE J, 10(04) (2005) 475-84. SPE-90368-PA.
[43] D. Wildenschild, A.P. Sheppard, X-ray imaging and analysis techniques for quantifying pore-scale structure and processes in subsurface porous medium systems, Adv. Water Resour. 51 (2013) 217–246.
[44] S. Iglauer, S. Favretto, G. Spinelli, G. Schena, M.J. Blunt, X-ray tomography measurements of power-law cluster size distributions for the nonwetting phase in sandstones, Phys. Rev. E 82 (5) (2010) 056315.
[45] M.J. Blunt, B. Bijeljic, H. Dong, O. Gharbi, S. Iglauer, P. Mostaghimi, et al., Pore-scale imaging and modelling, Adv. Water Resour. 51 (2013) 197–216.
[46] M. Andrew, B. Bijeljic, M.J. Blunt, Pore-scale imaging of geological carbon dioxide storage under in situ conditions, Geophys. Res. Lett. 40 (15) (2013) 3915–3918.
[47] S. Schlüter, A. Sheppard, K. Brown, D. Wildenschild, Image processing of multiphase images obtained via X-ray microtomography: a review, Water Resour. Res. 50 (4) (2014) 3615–3639.
[48] A.M. Alhammadi, A. AlRatrout, B. Bijeljic, M.J. Blunt, Pore-scale imaging and characterization of hydrocarbon reservoir rock wettability at subsurface conditions using X-ray microtomography, J. Visual. Exp.: JoVE. 140 (2018).
[49] E.V. Lebedeva, A. Fogden, Micro-CT and Wettability Analysis of Oil Recovery from Sand Packs and the Effect of Waterflood Salinity and Kaolinite, Energy Fuels 25 (12) (2011) 5683–5694.
[50] W. Bartels, M. Rücker, S. Berg, H. Mahani, A. Georgiadis, N. Brussee, et al., Micro-ct study of the impact of low salinity waterflooding on the pore-scale fluid distribution during flow, in: International Symposium of the Society of Core Analysts, Snowmass, CO. 22 (2016) 1362-73.
[51] M. Khishvand, A. Alizadeh, I.O. Kohshour, M. Piri, R. Prasad, In situ characterization of wettability alteration and displacement mechanisms governing recovery enhancement due to low-salinity waterflooding, Water Resour. Res. 53 (5) (2017) 4427–4443.
[52] M. Shabaninejad, J. Middlelton, A. Fogden, Systematic pore-scale study of low salinity recovery from Berea sandstone analyzed by micro-CT, J. Petrol. Sci. Eng. 163 (2018) 283–294.
[53] E. Andrews, A. Muggeridge, G. Garfi, A. Jones, S. Krevor, Pore-Scale X-ray Imaging of Wetting Alteration and Oil Redistribution during Low-Salinity Flooding of Berea Sandstone, Energy Fuels 35 (2) (2021) 1197–1207.
[54] W.-B. Bartels, M. Rücker, S. Berg, H. Mahani, A. Georgiadis, A. Fadili, et al., Fast X-Ray Micro-CT Study of the Impact of Brine Salinity on the Pore-Scale Fluid Distribution During Waterflooding, Petrophysics - SPWLA J. Form. Eval. Reserv. Descr. 58 (01) (2017) 36–47.
[55] Mirchi V, Pore-Scale Investigation of the Effect of Surfactant on Fluid Occupancies during Low-Salinity Waterflooding in Oil-Wet Carbonates. SPE Annual Technical Conference and Exhibition; Dallas, Texas, USA, September 2018. SPE-194045-STU.
[56] M. Tawfik, Z. Karpyn, R. Johns, Multiscale study of chemically-tuned waterflooding in carbonate rocks using micro-computed tomography, IOR 2019–20th European Symposium on Improved Oil Recovery; 2019: European Association of Geoscientists & Engineers.
[57] Z. Qin, M. Arshadi, M. Piri, Micro-scale experimental investigations of multiphase flow in oil-wet carbonates. I. In situ wettability and low-salinity waterflooding, Fuel 257 (2019) 116014.
[58] Selem AM, Agenet N, Blunt MJ, Bijeljic B. Pore-Scale Imaging of Tertiary Low Salinity Waterflooding in a Heterogeneous Carbonate Rock at Reservoir Conditions. SPE Annual Technical Conference and Exhibition; Dubai, UAE, September 2021. SPE-206357-MS.
[59] B. Bijeljic, P. Mostaghimi, M.J. Blunt, Insights into non-Fickian solute transport in carbonates, Water Resour. Res. 49 (5) (2013) 2714–2728.
[60] N. Alyafei, M.J. Blunt, The effect of wettability on capillary trapping in carbonates, Adv. Water Resour. 90 (2016) 36–50.
[61] Q. Lin, Y. Al-Khulaifi, M.J. Blunt, B. Bijeljic, Quantification of sub-resolution porosity in carbonate rocks by applying high-salinity contrast brine using X-ray microtomography differential imaging, Adv. Water Resour. 96 (2016) 306–322.
[62] A. Buades, B. Coll, J. Morel, A non-local algorithm for image denoising, in: 2005 IEEE Computer Society Conference on Computer Vision and Pattern Recognition (CVPR'05) 2 (2005) 60-5.
[63] M. Andrew, B. Bijeljic, M.J. Blunt, Pore-scale contact angle measurements at reservoir conditions using X-ray microtomography, Adv. Water Resour. 68 (2014) 24–31.
[64] A.C. Jones, C.H. Arns, A.P. Sheppard, D.W. Hutmacher, B.K. Milthorpe, M.A. Knackstedt, Assessment of bone ingrowth into porous biomaterials using MICRO-CT, Biomaterials 28 (15) (2007) 2491–2504.
[65] A. AlRatrout, A.Q. Raeini, B. Bijeljic, M.J. Blunt, Automatic measurement of contact angle in pore-space images, Adv. Water Resour. 109 (2017) 158–169.
[66] R.T. Armstrong, M.L. Porter, D. Wildenschild, Linking pore-scale interfacial curvature to column-scale capillary pressure, Adv. Water Resour. 46 (2012) 55–62.
[67] M. Andrew, B. Bijeljic, M.J. Blunt, Pore-scale imaging of trapped supercritical carbon dioxide in sandstones and carbonates, Int. J. Greenhouse Gas Control 22 (2014) 1–14.
[68] C. Sun, J.E. McClure, P. Mostaghimi, A.L. Herring, D.E. Meisenheimer, D. Wildenschild, et al., Characterization of wetting using topological principles, J. Colloid Interface Sci. 578 (2020) 106–115.
[69] H. Dong, M.J. Blunt, Pore-network extraction from micro-computerized-tomography images, Phys. Rev. E 80 (3) (2009) 036307.
[70] A.Q. Raeini, B. Bijeljic, M.J. Blunt, Generalized network modeling: Network extraction as a coarse-scale discretization of the void space of porous media, Phys. Rev. E 96 (1) (2017) 013312.
[71] Y. Gao, A.Q. Raeini, M.J. Blunt, B. Bijeljic, Pore occupancy, relative permeability and flow intermittency measurements using X-ray micro-tomography in a complex carbonate, Adv. Water Resour. 129 (2019) 56–69.
[72] Y. Gao, A.Q. Raeini, A.M. Selem, I. Bondino, M.J. Blunt, B. Bijeljic, Pore-scale imaging with measurement of relative permeability and capillary pressure on the same reservoir sandstone sample under water-wet and mixed-wet conditions, Adv. Water Resour. 146 (2020) 103786.
[73] A. Scanziani, K. Singh, T. Bultreys, B. Bijeljic, M.J. Blunt, In situ characterization of immiscible three-phase flow at the pore scale for a water-wet carbonate rock, Adv. Water Resour. 121 (2018) 446–455.
[74] R. Salathiel, Oil recovery by surface film drainage in mixed-wettability rocks, JPT 25(10) (1973) 1216-1224.
[75] Q. Lin, T. Akai, M.J. Blunt, B. Bijeljic, H. Iwama, K. Takabayashi, et al., Pore-scale imaging of asphaltene-induced pore clogging in carbonate rocks, Fuel 283 (2021) 118871.
[76] G. Taubin, Curve and surface smoothing without shrinkage, in: Proceedings of IEEE international conference on computer vision; 1995: IEEE.
[77] A.M. Alhammadi, Y. Gao, T. Akai, M.J. Blunt, B. Bijeljic, Pore-scale X-ray imaging with measurement of relative permeability, capillary pressure and oil recovery in a mixed-wet micro-porous carbonate reservoir rock, Fuel 268 (2020) 117018.
[78] A.M. Alhammadi, A. AlRatrout, K. Singh, B. Bijeljic, M.J. Blunt, In situ characterization of mixed-wettability in a reservoir rock at subsurface conditions, Sci. Rep. 7 (1) (2017) 10753.
[79] Q. Lin, B. Bijeljic, S. Berg, R. Pini, M.J. Blunt, S. Krevor, Minimal surfaces in porous media: Pore-scale imaging of multiphase flow in an altered-wettability Bentheimer sandstone, Phys. Rev. E 99 (6) (2019) 063105.
[80] K.F. Gauss, P. Pesic, General investigations of curved surfaces, Courier Corporation (2005).
[81] M. Berger, B. Gostiaux, Differential Geometry: Manifolds, Curves, and Surfaces: Manifolds, Curves, and Surfaces (Vol. 115), Springer Science & Business Media, 2012.
[82] I.D. Piñerez Torrijos, T. Puntervold, S. Strand, T. Austad, H.I. Abdullah, K. Olsen, Experimental Study of the Response Time of the Low-Salinity Enhanced Oil Recovery Effect during Secondary and Tertiary Low-Salinity Waterflooding, Energy Fuels 30 (6) (2016) 4733–4739.
[83] P. Mahzari, M. Sohrabi, A.J. Cooke, A. Carnegie, Direct pore-scale visualization of interactions between different crude oils and low salinity brine, J. Petrol. Sci. Eng. 166 (2018) 73–84.